

Sampled-Data Observer Based Dynamic Surface Control of Delayed Neuromuscular Functional Electrical Stimulation

Qiang Zhang, Ashwin Iyer, Ziyue Sun, Albert Dodson, and Nitin Sharma*

Neuromuscular Control and Robotics Lab
UNC & NC State Joint Department of Biomedical Engineering
NC State University
Raleigh, NC, 27695 USA

Email: qzhang25@ncsu.edu, aiyer3@ncsu.edu, zsun32@ncsu.edu, aedodson@ncsu.edu, and nsharm23@ncsu.edu

ABSTRACT

Functional electrical stimulation (FES) is a potential technique for reanimating paralyzed muscles post neurological injury/disease. Several technical challenges including difficulty in measuring and compensating for delayed muscle activation levels inhibit its satisfactory control performance. In this paper, an ultrasound (US) imaging approach is proposed to measure delayed muscle activation levels under the implementation of FES. Due to low sampling rates of US imaging, a sampled-data observer (SDO) is designed to estimate the muscle activation in a continuous manner. The SDO is combined with continuous-time dynamic surface control (DSC) approach that compensates for the electromechanical delay (EMD) in the tibialis anterior (TA) activation dynamics. The stability analysis based on the Lyapunov-Krasovskii function proves that the SDO-based DSC plus delay compensation (SDO-DSC-DC) approach achieves semi-global uniformly ultimately bounded (SGUUB) tracking performance. Simulation results on an ankle dorsiflexion neuromusculoskeletal system show the root mean square error (RMSE) of desired trajectory tracking is reduced by 19.77 % by using the proposed SDO-DSC-DC compared to the DSC-DC without the SDO. The findings provide potentials for rehabilitative devices, like powered exoskeleton and FES, to assist or enhance human limb movement based on the corresponding muscle activities in real-time.

Keywords: Functional electrical stimulation, Sampled-data observer, Dynamic surface control, Ankle dorsiflexion, Ultrasound imaging.

1. INTRODUCTION

Ankle dorsiflexion has a critical role in both human balance and walking [1, 2]. Therefore, a weakened function of ankle dorsiflexion impairs gait of affected persons. Drop foot is a typical symptom of weakened ankle dorsiflexion after cerebral vascular accidents and due to neurological disorders such as multiple sclerosis [3, 4]. Affected persons are unable to exhibit normal foot ground clearance during the swing phase, resulting in unnatural steppage gait to avoid tripping/falls [5]. To correct drop foot, functional electrical stimulation (FES), which is an artificial technique to apply electrical potentials across skeletal muscles, can be applied on the tibialis anterior (TA) muscle. Since the earlier demonstration of FES to correct drop foot by Kantowitz et al. [6] and Liberson et al. [7], recent studies [8, 9] have started its efficacy on a larger clinical population. Typically the TA muscle is artificially activated during the swing phase using discrete sensors that either detect heel contact or leg inclination [8]. The applied stimulation is fixed in amplitude or used a fixed pattern, e.g., trapezoid shape [10]. Although these studies implement event triggered control, their inability to modulate stimulation amplitude is a major drawback, given the nonlinear and time-varying nature of FES.

Closed-loop FES control can provide robust performance and recreate precise and accurate functional movements, e.g., walking [11, 12]. However, electromechanical delay (EMD) imposes a major challenge in designing closed-loop FES control. To address EMD, nonlinear delay compensation (DC) control methods have recently been proposed [13–15]. However, these

control methods were designed by considering only the second-order musculoskeletal dynamics, thereby neglecting the muscle activation dynamics. In [16], to account for the EMD and activation dynamics, a proportional-derivative (PD) controller using a dynamic surface control (DSC) error structure along with a DC term was developed. However, the control design was based on the assumption that the muscle activation variable is measurable in real-time. To address the hard-to-measure muscle activation dynamics, the authors then proposed a model-based estimator to predict the muscle activation levels [17]. The model-based estimator was parameterized by using off-line system identification [18] before performing the controller in tracking experiments, and there was no muscle physiological state feedback during the experiments.

Motivation exists to use direct measurement of FES-induced muscle activation and thus enable FES control based on a more accurate (third-order) musculoskeletal dynamics. Surface electromyography (sEMG) can be used to represent muscle activation [19], but due to the presence of stimulation artifacts [20] and noise interference, sEMG is an unreliable sensing technique for measuring muscle activation. Recently, ultrasound (US) imaging has been proposed as an alternative non-invasive technology to directly visualize skeletal muscle contractility. For example, Zhang et al. [21] combined sEMG signal-induced and US imaging structural features-induced muscle activation levels to predict volitional isometric ankle dorsiflexion effort based on a modified Hill-type neuromuscular model. In [22], an adaptive speckle tracking algorithm to detect the quadriceps contraction strain by using US imaging was proposed to quantitatively evaluate muscle fatigue induced by FES. Compared to sEMG, the structural and functional features of US imaging are not affected by stimulation artifacts during FES.

In this paper, we propose to use US imaging to detect FES-induced muscle activation levels during an ankle trajectory tracking task. One of the main challenges is that US image generation and processing algorithms are computationally intensive. Most studies process US data offline to investigate muscle contractility changes due to FES, thus, the real-time use of US data to monitor muscle activity and aid control performance will be pioneering for FES control. Towards this goal, we assume that US data is available for closed-loop control, although at a much lower sampling frequency compared to other kinematic measurements, like signals from inertia measurement units (IMU) or incremental encoders. Therefore, given the US derived signal at a lower sampling rate, a sampled-measurement data based observer (SDO) is proposed to estimate the TA muscle activation level in a continuous manner, which meets the control requirements of a continuous state feedback.

Contributions on SDO design have been proposed in recent years. For example, Shen et al. [23] proposed a continuous observer for a class of multi-output nonlinear systems with multi-rate sampled and delayed output measurements, where the ob-

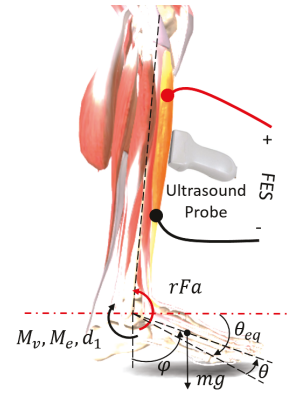


FIGURE 1. THE SCHEMATIC OF FES-INDUCED ANKLE DORSIFLEXION SETUP. NOTICE THAT ONLY THE TIBIALIS ANTERIOR IS BEING STIMULATED MEANING THAT FES CAN ONLY PRODUCE ANKLE DORSIFLEXION AND GRAVITY IS RELIED IN TO MOVE THE FOOT BACK TO THE EQUILIBRIUM POINT θ_{eq} .

servator error was proven to be globally exponentially stable. In our previous work [24], for a volitional ankle neuromusculoskeletal system, a continuous observer was designed based on multi-rate and delayed measurements from US imaging and IMUs. Further studies on SDO-based control for nonlinear systems have also been proposed in recent years [25–27]. In [28], the authors investigated the problem of output feedback stabilization with a linear continuous-discrete observer for a class of upper-triangular nonlinear system based on sampled and delayed single measurement. However, the aforementioned SDO-based control techniques mainly focused on regulation or stabilization task, and few contributions have been proposed for trajectory tracking task.

In this paper, the continuously estimated muscle activation levels from SDO, based on sampled US imaging measurement, is combined with a newly designed proportional-integral-derivative (PID) type DSC-DC controller to perform ankle dorsiflexion tracking task. The proposed SDO based PID-DSC-DC controller is compared with a PID-DSC-DC controller with the pure solution of muscle activation dynamics using the offline identified model parameters.

2. ANKLE DORSIFLEXION SYSTEM MODEL AND OBSERVER MODEL

The dynamic model of the FES-induced ankle dorsiflexion movement, as shown in Fig. 1, is given as

$$J\ddot{\theta} + M_v + M_e + M_g + d_1 = \tau \quad (1)$$

where $J \in \mathbb{R}^+$ is the unknown inertia term of the foot along the dorsiflexion rotation center axis, $\theta(t) \in \mathbb{R}$, $\dot{\theta}(t) \in \mathbb{R}$, and

$\ddot{\theta}(t) \in \mathbb{R}$ denote the angular position, angular velocity, and angular acceleration of the ankle dorsiflexion, respectively. The constant ankle equilibrium point is represented as $\theta_{eq} \in \mathbb{R}^+$, which is the position that the foot is completely relaxed. The passive moment $M_v(\dot{\theta}) \in \mathbb{R}$ represents musculoskeletal viscosity, $M_e(\theta) \in \mathbb{R}$ represents musculoskeletal elasticity, and $M_g(\theta) = mgl \sin(\frac{\pi}{2} + \theta - \theta_{eq}) \in \mathbb{R}$ is the gravitational term acting on the ankle. The mass of the foot and the length from foot's center of mass to the ankle rotation center are denoted as $m \in \mathbb{R}^+$ and $l \in \mathbb{R}^+$. The explicit definitions of the functions, $M_v(\dot{\theta})$ and $M_e(\theta)$, can be obtained from [29, 30]. The term related to modeling uncertainties and external disturbance is denoted as $d_1(t) \in \mathbb{R}$. FES-induced ankle dorsiflexion torque is denoted as $\tau(t) \triangleq r(\theta)F(\theta, \dot{\theta})a(t) \in \mathbb{R}$, where the positive moment arm for the TA is denoted as $r(\theta) \in \mathbb{R}^+$. $F(\theta, \dot{\theta})$ denotes the nonlinear relationship of muscle force-fascicle length and muscle force-fascicle velocity [21], and $a(t) \in [0, 1]$ is the muscle activation level whose dynamics is represented by the following continuous differential equation

$$\dot{a} = \frac{-a + u(t - \tau_M)}{T_a} + d_2. \quad (2)$$

In (2), $\tau_M \in \mathbb{R}^+$ is the EMD caused by FES and is assumed to be known, $T_a \in \mathbb{R}^+$ is the muscle activation decay constant, and $d_2(t) \in \mathbb{R}$ is the modeling uncertainties and disturbance in the muscle activation model. The normalized FES input $u(t) \in [0, 1]$ is due to the boundedness of the muscle stimulation. From [31], $u(t)$ is modeled by a piece-wise linear function

$$u(t) = \begin{cases} 0 & \bar{u} < u_{\min} \\ \frac{\bar{u}(t) - u_{\min}}{u_{\max} - u_{\min}} & u_{\min} \leq \bar{u} \leq u_{\max} \\ 1 & \bar{u} > u_{\max} \end{cases} \quad (3)$$

where u_{\min} and $u_{\max} \in \mathbb{R}_{\geq 0}$ are the stimulation threshold and stimulation saturation, respectively, and $\bar{u}(t) \in \mathbb{R}_{\geq 0}$ is the stimulation current amplitude applied on the muscle.

To facilitate the control development and stability analysis, the musculoskeletal system dynamics in (1) are rewritten to a state space form as

$$\dot{x} = \begin{bmatrix} x_2 \\ -J_{\Gamma}^{-1}(M_{\Gamma_v} + M_{\Gamma_e} + M_{\Gamma_g} + d_{\Gamma_1} - x_3) \\ -\frac{x_3}{T_a} + \frac{u(t - \tau_M)}{T_a} + d_2 \end{bmatrix} \quad (4)$$

where $x = [\theta, \dot{\theta}, a]^T$, $\Gamma = rF$, $J_{\Gamma} = \frac{J}{\Gamma}$, $M_{\Gamma_v} = \frac{M_v}{\Gamma}$, $M_{\Gamma_e} = \frac{M_e}{\Gamma}$, $M_{\Gamma_g} = \frac{M_g}{\Gamma}$, and $d_{\Gamma_1} = \frac{d_1}{\Gamma}$. In the meanwhile, the measurement model is also given as

$$y = \begin{bmatrix} x_1(t) \\ x_2(t) \\ x_3(t_k) \end{bmatrix}, k = 0, 1, 2, \dots \quad (5)$$

where angular position θ and velocity $\dot{\theta}$ are measurable by using IMU or encoders with high sampling frequency, so they satisfy the requirement as feedback signals in real-time. The muscle activation a is measurable by using normalized variables, like pennation angle, fascicle length, and echogenicity from US imaging [21], but with much lower sampling frequency due to the computationally intensive image processing. The US imaging-derived muscle activation signals are available at discrete instant t_k , and $\{t_k\}$ is a monotonically increasing sequence and satisfies $\lim_{k \rightarrow \infty} t_k = \infty$. The sampling interval is assumed as a positive constant value T , including the elapsed time on US image generation and processing.

The following assumptions are given to finalize the observer and controller design.

Assumption 1: The nonlinear functions $r(\theta)$ and $F(\theta, \dot{\theta})$ are assumed to be nonzero, positive, bounded functions, and their first-order and second-order time derivative exist and are bounded. Therefore, Γ is also a nonzero, positive, and bounded function, and the first-order and second-order time derivative exist and are bounded.

Assumption 2: The modeling uncertainties and disturbance d_1 in (1) and d_2 in (2) are bounded, and their first-order and second-order time derivative exist and are bounded. So based on Assumption 1, d_{Γ_1} is also assumed to be bounded and its first-order and second-order time derivative exist and are bounded.

Assumption 3: Based on Assumption 1, the term J_{Γ} is bounded and its first-order and second-order time derivative exist and are bounded.

Assumption 4: The desired ankle trajectory $\theta_d \in \mathbb{R}$ and its time derivatives, $\dot{\theta}_d$ and $\ddot{\theta}_d$, are bounded.

To fulfill the goal of continuous muscle activation feedback, the proposed SDO for TA muscle activation in (5) during $t \in [t_k, t_{k+1})$ is given by

$$\dot{\hat{x}}_3(t) = -\frac{\hat{x}_3(t)}{T_a} + \frac{u(t - \tau_M)}{T_a} + \gamma \varepsilon_3(t_k) \quad (6)$$

where γ is a positive observation gain that will be subsequently constrained in stability analysis section. $\varepsilon_3(t_k) = \hat{x}_3(t_k) - x_3(t_k)$ is a constant value during the time interval $t \in [t_k, t_{k+1})$, will be updated at every time point when the US imaging-derived normalized variable is available, and it is assumed to be bounded. Therefore, the observer model is of a hybrid nature with continuous and discrete variables. By taking the error between the

continuous muscle activation dynamics in (4) and the SDO in (6), the observation error dynamics is given as

$$\dot{\varepsilon}_3(t) = -\frac{\varepsilon_3(t)}{T_a} + \gamma\varepsilon_3(t_k) - d_2(t). \quad (7)$$

3. CONTROL DEVELOPMENT WITH SDO

The objective of this paper is to develop a trajectory tracking controller for FES-actuated ankle neuromusculoskeletal system that considers the continuous muscle activation and the EMD in the FES system. This will be achieved by designing a PID controller that uses a DSC framework along with a SDO to address hard-to-measure problem for muscle activation. In addition, a delay compensation (DC) term is added to address the FES-induced EMD problem in TA activation dynamics.

The trajectory tracking error for the proposed closed-loop control system is given as

$$e(t) = x_d(t) - x_1(t) \quad (8)$$

where $x_d(t) \in \mathbb{R}$ is the desired continuously differentiable ankle dorsiflexion trajectory. For facilitating control design and stability analysis, the following two auxiliary error signals $e_1(t)$ and $e_2(t) \in \mathbb{R}$ are defined as

$$\begin{aligned} e_1(t) &= \dot{e}_0(t) + \alpha_0 e_0(t) \\ e_2(t) &= \dot{e}_1(t) + \alpha_1 e_1(t) \end{aligned} \quad (9)$$

where α_0 and $\alpha_1 \in \mathbb{R}^+$ are control gains and $e_0(t)$ is another auxiliary error signal to incorporate integral control, which is defined as

$$e_0(t) = \int_0^t e(s) ds. \quad (10)$$

After taking the time derivative of $e_2(t)$, multiplying with J_Γ , and using (4), (8)-(10), we get

$$J_\Gamma \dot{e}_2 = J_\Gamma \ddot{x}_d + f_\Gamma + d_{\Gamma 1} - x_3 + J_\Gamma(\alpha_0 + \alpha_1)\dot{e} + J_\Gamma \alpha_0 \alpha_1 e \quad (11)$$

where $f_\Gamma = M_{\Gamma v} + M_{\Gamma e} + M_{\Gamma g}$. Assume the desired differentiable TA muscle activation signal as $x_{3d} \in \mathbb{R}_{\geq 0}$, then the surface error is defined as

$$S = x_{3d} - \hat{x}_3. \quad (12)$$

By adding and subtracting x_{3d} , \hat{x}_3 , and a DC term, $e_I \in \mathbb{R}$, multiplied by a constant gain $\delta \in \mathbb{R}^+$, where $e_I(t) = \int_{t-\tau_M}^t u(s) ds$ in (11), the rearranged format of (11) can be given as

$$J_\Gamma \dot{e}_2 = -\frac{1}{2} J_\Gamma e_2 + S - \delta e_I + \varepsilon_3 + \tilde{\mathcal{H}} + \mathcal{O} - x_{3d} - e_1 \quad (13)$$

where the auxiliary signals $\tilde{\mathcal{H}}(e, e_1, e_2, e_I, x_d, \dot{x}_d, \ddot{x}_d, t) \in \mathbb{R}$ and $\mathcal{O}(x_d, \dot{x}_d, \ddot{x}_d, \Gamma, t) \in \mathbb{R}$ are defined as

$$\begin{aligned} \tilde{\mathcal{H}} &= \mathcal{H} - \mathcal{H}_d, \quad \mathcal{O} = d_{\Gamma 1} + \mathcal{H}_d \\ \mathcal{H} &= \frac{1}{2} J_\Gamma e_2 + J_\Gamma \dot{x}_d + f_\Gamma + \delta e_I + e_1 \\ &\quad + J_\Gamma(\alpha_0 + \alpha_1)\dot{e} + J_\Gamma \alpha_0 \alpha_1 e \\ \mathcal{H}_d &= J_\Gamma \ddot{x}_d + f_\Gamma(x_d, \dot{x}_d) \end{aligned} \quad (14)$$

where $J_{\Gamma d} = \frac{J}{r(x_d)F(x_d, \dot{x}_d)}$ and $f_\Gamma(x_d, \dot{x}_d) = \frac{M_v(\dot{x}_d) + M_e(x_d) + M_g(x_d)}{r(x_d)F(x_d, \dot{x}_d)}$. Furthermore, according to the Assumptions 1-4, the two auxiliary signals $\tilde{\mathcal{H}}$ and \mathcal{O} can be bounded as

$$|\tilde{\mathcal{H}}| \leq \rho(\|z\|)\|z\|, \quad |\mathcal{O}| \leq \zeta. \quad (15)$$

where $\zeta \in \mathbb{R}^+$ is a known constant, $\rho(\|z\|) \in \mathbb{R}^+$ is a positive globally invertible non-decreasing function, and $z(e, e_0, e_1, e_2, e_I) \in \mathbb{R}^5$ is defined as

$$z = [e, e_0, e_1, e_2, e_I]^T. \quad (16)$$

In the expression (13), the desired muscle activation is defined as [17]

$$x_{3d} = ke_2 = k\dot{e} + (\alpha_0 + \alpha_1)ke + k\alpha_0\alpha_1e_0 \quad (17)$$

where $k = k_1 + k_2 + k_3 \in \mathbb{R}^+$, which implies a PID type signal with three different control gains, and the corresponding coefficients are defined as $k_p = (\alpha_0 + \alpha_1)k$, $k_d = k$, and $k_i = k\alpha_0\alpha_1$.

By using the definition in (17), the formula (13) can be rewritten as

$$J_\Gamma \dot{e}_2 = -\frac{1}{2} J_\Gamma e_2 + S_n + \varepsilon_3 + \tilde{\mathcal{H}} + \mathcal{O} - ke_2 - e_1 \quad (18)$$

where $S_n = S - \delta e_I$, which is the augmented surface error that contains the DC term δe_I . By substituting (12) and (6), the time derivative of S_n is given as

$$\dot{S}_n = \dot{\phi} + \frac{\hat{x}_3}{T_a} + \left(\delta - \frac{1}{T_a} \right) u(t - \tau_M) - \delta u(t) - \gamma\varepsilon_3(t_k) \quad (19)$$

where $\phi = \frac{d}{dt}(ke_2)$. The DC term e_I is proposed to replace the delayed input in the muscle activation dynamics with a non-delayed input. By manipulating the non-delayed input, which is defined as the control law $u(t)$ as

$$u(t) = \frac{1}{\delta} [\beta S_n + \phi] \quad (20)$$

where $\beta \in \mathbb{R}^+$ is a control gain, we can get the closed-loop surface error dynamics as below

$$\dot{S}_n = -\beta S_n + \frac{\dot{x}_3}{T_a} + \left(\delta - \frac{1}{T_a} \right) u(t - \tau_M) - \gamma \epsilon_3(t_k). \quad (21)$$

4. STABILITY ANALYSIS

Lemma 1. For any given positive definite matrix $M \in \mathbb{R}^{n \times n}$, a positive scalar α , and a vector function v , the following Cauchy Schwarz inequality always holds as

$$\left[\int_0^\alpha v(s) ds \right]^T M \left[\int_0^\alpha v(s) ds \right] \leq \alpha \left[\int_0^\alpha v^T(s) M v(s) ds \right]. \quad (22)$$

The proof for this Lemma can be found in [32].

Theorem 1. Consider the neuromusculoskeletal system in (4) with a known input delay, by using the sampled US imaging-based observer for TA muscle activation in (6) and control law in (20), the ankle dorsiflexion trajectory tracking error is ensured to be semi-globally uniformly ultimately bounded (SGUUB) provided that the observer gain γ and control gains α_0 , α_1 , k_1 , k_2 , β , and δ satisfy the following sufficient conditions:

$$\begin{aligned} & \alpha_0 \geq \frac{1}{2}, \alpha_1 \geq \frac{1}{2}, k_1 \geq 1, \\ & \beta \geq \frac{1}{2} \left[\tau_M + \frac{1}{2} + \gamma + \frac{\psi^2}{2\epsilon} + \sqrt{\left(\tau_M + \frac{1}{2} + \gamma + \frac{\psi^2}{2\epsilon} \right)^2 + 4\tau_M} \right], \\ & 0 < \gamma \leq \frac{1}{2T_a} - \frac{1}{2}, \kappa \geq \frac{3\gamma T}{T_a^2}, \\ & k_2 \geq \frac{\rho^2(\|z\|)}{4 \min\left\{ \alpha_0 - \frac{1}{2}, \alpha_1 - \frac{1}{2}, k_1 - 1, \frac{\delta^2}{2\tau_M \beta^2} \right\}} \end{aligned}$$

where τ_M is the EMD, γ is the observation update gain, ϵ is a arbitrary positive constant, ψ and κ are positive constant values defined in the subsequent stability analysis.

Proof: Define an augmented vector $w(t) \in \mathbb{R}^6$ as

$$w = \left[e_0, e_1, e_2, S_n, \epsilon_3, \sqrt{P} \right]^T.$$

A positive definite continuously differentiable functional $V_1(w, t) : \mathcal{L} \times [t_0, \infty) \rightarrow \mathbb{R}^+$ is defined as

$$V_1(w, t) \triangleq \frac{1}{2} (e_0^2 + e_1^2 + J_T e_2^2 + S_n^2 + \epsilon_3^2) + P \quad (23)$$

and $V_1(w, t)$ can be bounded as

$$\underline{\lambda} \|w\|^2 \leq V_1 \leq \bar{\lambda} \|w\|^2 \quad (24)$$

where $\underline{\lambda}$ and $\bar{\lambda} \in \mathbb{R}$ are two positive constants that is used to bound the Lyapunov functional candidate. Additionally, the Lyapunov-Krasovskii functional $P \in \mathbb{R}^+$ in (23) is defined as

$$P = \frac{\delta^2}{\beta^2} \int_{t-\tau_M}^t \left(\int_s^t u(\omega)^2 d\omega \right) ds. \quad (25)$$

Taking the time derivative of (23) and using (7), (9), (10), (18), and (21) will result in the following expression

$$\begin{aligned} \dot{V}_1 = & -\alpha_0 e_0^2 - \alpha_1 e_1^2 - ke_2^2 + e_2 (S_n + \epsilon_3 + \mathcal{H} + \mathcal{O}) \\ & + e_0 e_1 - \frac{1}{T_a} \epsilon_3^2 + \gamma \epsilon_3^2 - \gamma \epsilon_3 (\epsilon_3 - \epsilon_3(t_k)) - \epsilon_3 d_2 \\ & + S_n \left[\frac{\dot{x}_3}{T_a} + \left(\delta - \frac{1}{T_a} \right) u(t - \tau_M) - \gamma \epsilon_3(t_k) \right] \\ & - \beta S_n^2 + \frac{\delta^2}{\beta^2} \tau_M u^2 - \frac{\delta^2}{\beta^2} \int_{t-\tau_M}^t u(s)^2 ds. \end{aligned} \quad (26)$$

In the time interval $t \in [t_k, t_{k+1})$, by substituting $\int_{t_k}^t \dot{\epsilon}_3(s) ds = \epsilon_3(t) - \epsilon_3(t_k)$ to (26), and substituting $u(t)$ in (20) to (26), the following equation results in

$$\begin{aligned} \dot{V}_1 = & -\alpha_0 e_0^2 - \alpha_1 e_1^2 - ke_2^2 + e_2 (S_n + \epsilon_3 + \mathcal{H} + \mathcal{O}) \\ & + e_0 e_1 - \frac{1}{T_a} \epsilon_3^2 + \gamma \epsilon_3^2 - \gamma \epsilon_3 \int_{t_k}^t \dot{\epsilon}_3(s) ds - \epsilon_3 d_2 \\ & + S_n \left[\frac{\dot{x}_3}{T_a} + \left(\delta - \frac{1}{T_a} \right) u(t - \tau_M) - \gamma \epsilon_3 \right] - \beta S_n^2 \\ & + \gamma S_n \int_{t_k}^t \dot{\epsilon}_3(s) ds + \tau_M S_n^2 + \frac{\tau_M}{\beta^2} \phi^2 + \frac{2\tau_M}{\beta} S_n \phi \\ & - \frac{\delta^2}{\beta^2} \int_{t-\tau_M}^t u(s)^2 ds. \end{aligned} \quad (27)$$

Based on Young's inequality, Assumption 1-3, the following terms will be bounded as

$$\begin{aligned} |e_0| |e_1| & \leq \frac{1}{2} (e_0^2 + e_1^2), |e_2| |S_n| \leq \frac{1}{2} (e_2^2 + S_n^2) \\ |e_2| |\epsilon_3| & \leq \frac{1}{2} (e_2^2 + \epsilon_3^2), |\epsilon_3| |S_n| \leq \frac{1}{2} (\epsilon_3^2 + S_n^2) \\ |\epsilon_3| |d_2| & \leq \frac{1}{2} (\epsilon_3^2 + d_2^2), |\phi| |S_n| \leq \frac{1}{2} (S_n^2 + \phi^2) \\ |\epsilon_3| \left| \int_{t_k}^t \dot{\epsilon}_3(s) ds \right| & \leq \frac{1}{2} \left(\epsilon_3^2 + \left(\int_{t_k}^t \dot{\epsilon}_3(s) ds \right)^2 \right) \\ |S_n| \left| \int_{t_k}^t \dot{\epsilon}_3(s) ds \right| & \leq \frac{1}{2} \left(S_n^2 + \left(\int_{t_k}^t \dot{\epsilon}_3(s) ds \right)^2 \right) \\ |S_n| \left| \frac{\dot{x}_3}{T_a} + \left(\delta - \frac{1}{T_a} \right) u(t - \tau_M) \right| & \leq \psi |S_n| \leq \frac{\psi^2 S_n^2}{2\epsilon} + \frac{\epsilon}{2}. \end{aligned} \quad (28)$$

where $\bar{d}_2 \in \mathbb{R}^+$ is the upper bound magnitude of $d_2(t)$, $\varepsilon \in \mathbb{R}^+$ is an arbitrary constant, and $\psi \in \mathbb{R}^+$ is the upper bound of $\left| \frac{\xi_3}{T_a} + \left(\delta - \frac{1}{T_a} \right) u(t - \tau_M) \right|$. By applying the inequalities in (28), boundary conditions in (15), and Lemma 1, (27) can be further bounded as

$$\begin{aligned} \dot{V}_1 \leq & -\left(\alpha_0 - \frac{1}{2}\right) e_0^2 - \left(\alpha_1 - \frac{1}{2}\right) e_1^2 - \left(\frac{1}{T_a} - 2\gamma - 1\right) \varepsilon_3^2 \\ & - \left(\beta - \tau_M - \frac{1}{2} - \gamma - \frac{\tau_M}{\beta} - \frac{\psi^2}{2\varepsilon}\right) S_n^2 - (k_1 - 1) e_2^2 \\ & + |e_2| \zeta + |e_2| \rho (\|z\|) \|z\| + \frac{\varepsilon}{2} + \frac{\tau_M}{\beta^2} \phi^2 + \frac{\tau_M}{\beta} \phi^2 \\ & + \left(\frac{1}{2} + 3\gamma T^2\right) \bar{d}_2^2 - \frac{\delta^2}{\beta^2} \int_{t-\tau_M}^t u(s)^2 ds \\ & + 3\gamma^3 T^2 \varepsilon_3(t_k)^2 + \frac{3\gamma T}{T_a^2} \int_{t_k}^t \varepsilon_3(s)^2 ds. \end{aligned} \quad (29)$$

After adding and subtracting $\frac{\rho(\|z\|)\|z\|^2}{4k_2}$ and $\frac{\zeta^2}{4k_3}$, and recalling $k = k_1 + k_2 + k_3$, the further bounding result becomes

$$\begin{aligned} \dot{V}_1 \leq & -\left(\alpha_0 - \frac{1}{2}\right) e_0^2 - \left(\alpha_1 - \frac{1}{2}\right) e_1^2 - \left(\frac{1}{T_a} - 2\gamma - 1\right) \varepsilon_3^2 \\ & - \left(\beta - \tau_M - \frac{1}{2} - \gamma - \frac{\tau_M}{\beta} - \frac{\psi^2}{2\varepsilon}\right) S_n^2 - (k_1 - 1) e_2^2 \\ & + \frac{\rho(\|z\|)\|z\|^2}{4k_2} + \frac{\zeta^2}{4k_3} + \frac{\varepsilon}{2} + \frac{\tau_M}{\beta^2} \phi^2 + \frac{\tau_M}{\beta} \phi^2 \\ & + \left(\frac{1}{2} + 3\gamma T^2\right) \bar{d}_2^2 - \frac{\delta^2}{\beta^2} \int_{t-\tau_M}^t u(s)^2 ds \\ & + 3\gamma^3 T^2 \varepsilon_3(t_k)^2 + \frac{3\gamma T}{T_a^2} \int_{t_k}^t \varepsilon_3(s)^2 ds. \end{aligned} \quad (30)$$

Construct the following auxiliary integral functional, which is also positive definite continuously differentiable, as

$$V_2(t) = \int_{t-T}^t \int_{\rho} \varepsilon_3(s)^2 ds d\rho, t \in [t_0, \infty) \quad (31)$$

then (31) has an upper bound, which is given as

$$V_2(t) \leq T \int_{t-T}^t \varepsilon_3(s)^2 ds. \quad (32)$$

By taking the time derivative of (31), we have

$$\dot{V}_2 = T \varepsilon_3^2 - \int_{t-T}^t \varepsilon_3(s)^2 ds. \quad (33)$$

Now, consider the following Lyapunov-Krasovskii functional candidate

$$V(t) = V_1(w, t) + \kappa V_2(t). \quad (34)$$

where $\kappa \in \mathbb{R}^+$ is a constant. From (30), (32), and (33), we can obtain

$$\begin{aligned} \dot{V} \leq & -\left(\alpha_0 - \frac{1}{2}\right) e_0^2 - \left(\alpha_1 - \frac{1}{2}\right) e_1^2 - \left(\frac{1}{T_a} - 2\gamma - 1\right) \varepsilon_3^2 \\ & - \left(\beta - \tau_M - \frac{1}{2} - \gamma - \frac{\tau_M}{\beta} - \frac{\psi^2}{2\varepsilon}\right) S_n^2 - (k_1 - 1) e_2^2 \\ & + \frac{\rho(\|z\|)\|z\|^2}{4k_2} + \frac{\zeta^2}{4k_3} + \frac{\varepsilon}{2} + \frac{\tau_M}{\beta^2} \phi^2 + \frac{\tau_M}{\beta} \phi^2 \\ & + \left(\frac{1}{2} + 3\gamma T^2\right) \bar{d}_2^2 - \frac{\delta^2}{\beta^2} \int_{t-\tau_M}^t u(s)^2 ds \\ & + 3\gamma^3 T^2 \varepsilon_3(t_k)^2 + \kappa T \varepsilon_3^2 - \left(\kappa - \frac{3\gamma T}{T_a^2}\right) \int_{t-T}^t \varepsilon_3(s)^2 ds. \end{aligned} \quad (35)$$

Recall $e_I(t) = \int_{t-\tau_M}^t u(s) ds$, by using Lemma 1 again, we have

$$e_I^2(t) = \left(\int_{t-\tau_M}^t u(s) ds \right)^2 \leq \tau_M \int_{t-\tau_M}^t u(s)^2 ds. \quad (36)$$

Then by multiplying $-\frac{\delta^2}{2\tau_M\beta^2}$, the following inequality is given as

$$-\frac{\delta^2}{2\tau_M\beta^2} \left(\tau_M \int_{t-\tau_M}^t u(s)^2 ds \right) \leq -\frac{\delta^2}{2\tau_M\beta^2} e_I^2. \quad (37)$$

Therefore, (30) results in

$$\begin{aligned} \dot{V} \leq & -\left\{ \xi - \frac{\rho^2(\|z\|)}{4k_2} \right\} \|z\|^2 - \left(\frac{1}{T_a} - 2\gamma - 1 - \kappa T\right) \varepsilon_3^2 \\ & - \left(\beta - \tau_M - \frac{1}{2} - \gamma - \frac{\tau_M}{\beta} - \frac{\psi^2}{2\varepsilon}\right) S_n^2 + \frac{\zeta^2}{4k_3} + \vartheta \\ & - \frac{\delta^2}{2\beta^2} \int_{t-\tau_M}^t u(s)^2 ds + 3\gamma^3 T^2 \varepsilon_3(t_k)^2 \\ & - \left(\kappa - \frac{3\gamma T}{T_a^2}\right) \int_{t_k}^t \varepsilon_3(s)^2 ds. \end{aligned} \quad (38)$$

where $\xi = \min \left\{ \alpha_0 - \frac{1}{2}, \alpha_1 - \frac{1}{2}, k_1 - 1, \frac{\delta^2}{2\tau_M\beta^2} \right\}$ and $\vartheta = \sup_{\varepsilon_2} \left\{ \frac{\varepsilon}{2} + \frac{\tau_M}{\beta^2} \phi^2 + \frac{\tau_M}{\beta} \phi^2 + \left(\frac{1}{2} + 3\gamma T^2\right) \bar{d}_2^2 \right\}$. Given that

$$\int_{t-\tau_M}^t \left(\int_{\omega}^t u(\omega)^2 d\omega \right) ds \leq \tau_M \int_{t-\tau_M}^t u(s)^2 ds$$

(38) can be written as

$$\begin{aligned} \dot{V} \leq & -\left\{ \xi - \frac{\rho^2(\|z\|)}{4k_2} \right\} \|z\|^2 - \left(\frac{1}{T_a} - 2\gamma - 1 - \kappa T\right) \varepsilon_3^2 \\ & - \left(\beta - \tau_M - \frac{1}{2} - \gamma - \frac{\tau_M}{\beta} - \frac{\psi^2}{2\varepsilon}\right) S_n^2 + \frac{\zeta^2}{4k_3} + \vartheta \\ & - \frac{1}{2\tau_M} P + 6\gamma^3 T^2 V_1(t_k) - \left(\frac{\kappa}{T} - \frac{3\gamma}{T_a^2}\right) V_2. \end{aligned} \quad (39)$$

According to the definition of $z(t)$ and $w(t)$, (39) can be upper bounded as

$$\dot{V} \leq -\left\{ \xi - \frac{\rho^2(\|z\|)}{4k_2} \right\} \|e_I\|^2 - \bar{\xi} \|w\|^2 + \zeta - \left(\frac{\kappa}{T} - \frac{3\gamma}{T_a^2} \right) V_2 \quad (40)$$

where $\zeta = \frac{\tau^2}{4k_3} + \vartheta + 6\gamma^3 T^2 V_1(t_k)$, which is bounded by $\bar{\zeta} \in \mathbb{R}^+$, and $\bar{\xi}(\|z\|) \in \mathbb{R}^+$ is defined as

$$\bar{\xi}(\|z\|) = \min \left\{ \frac{1}{T_a} - 2\gamma - 1 - \kappa T, \xi - \frac{\rho^2(\|z\|)}{4k_2}, \beta - \tau_M - \frac{1}{2} - \gamma - \frac{\tau_M}{\beta} - \frac{\psi^2}{2\varepsilon}, \frac{1}{2\tau_M} \right\}.$$

The expression (40) can be further bounded when it satisfies the condition $\xi - \frac{\rho^2(\|z\|)}{4k_2} \geq 0$, which is true if the condition $\|z\|^2 \leq \rho^{-2} \left(2\sqrt{k_2} \bar{\xi} \right)$ is satisfied, which implies $\dot{V} \leq -\bar{\xi} \|w\|^2 + \bar{\zeta} - \left(\frac{\kappa}{T} - \frac{3\gamma}{T_a^2} \right) V_2$. Given the definition of z and w , a set for initial condition of the augmented vector $w(t)$ can be defined as

$$\mathcal{F} \triangleq \left\{ w(t) \in \mathbb{R}^6 \mid \|w(0)\| < \sqrt{\frac{\lambda}{\lambda} \left[\min \left\{ 1, \frac{\delta^2}{\tau\beta^2} \right\} \rho^{-2} \left(2\sqrt{k_2} \bar{\xi} \right) - \bar{\zeta} \right]} \right\}. \quad (41)$$

Based on the conditions in Theorem 1, $\bar{\xi}(\|z\|) \geq 0$ always holds and it can be lower bounded by a positive constant $\varpi \leq \bar{\xi}(\|z\|) \in \mathbb{R}_{\geq 0}$. Recall the upper bound of V_1 in (24), the inequality in (40) can be rewritten as

$$\begin{aligned} \dot{V} &\leq -\frac{\varpi}{\lambda} V_1 - \left(\frac{\kappa}{T} - \frac{3\gamma}{T_a^2} \right) V_2 + \bar{\zeta} \\ &\leq -\iota V + \bar{\zeta}. \end{aligned} \quad (42)$$

where ι is a positive value and defined as $\iota = \min \left\{ 1, \kappa, \frac{\varpi}{\lambda}, \frac{\kappa}{T} - \frac{3\gamma}{T_a^2} \right\}$. Therefore, for $w(0) \in \mathcal{F}$, the solution of the linear differential equation (42) is given as

$$V(t) \leq V(0)e^{-\iota t} + \frac{\bar{\zeta}}{\iota} (1 - e^{-\iota t}). \quad (43)$$

From (43), by providing the control gains $\alpha_0, \alpha_1, k_1, k_2, \beta$, and δ , as well as the observation gain γ according to the sufficient conditions in Theorem 1, $V(t)$ decays exponentially to a boundary $\frac{\bar{\zeta}}{\iota}$. Because $V \in \mathcal{L}_\infty$, the state variables in the augmented vector $e_0, e_1, e_2, S_n, \varepsilon_3, \sqrt{P} \in \mathcal{L}_\infty$. Recall the lower bound of V_1 in (24), further analysis can be done to show the ball radius of the $\|w\|$ convergence is $\sqrt{\frac{\bar{\zeta}}{\lambda \iota}}$. Therefore, we can conclude that the closed-loop system is SGUUB.

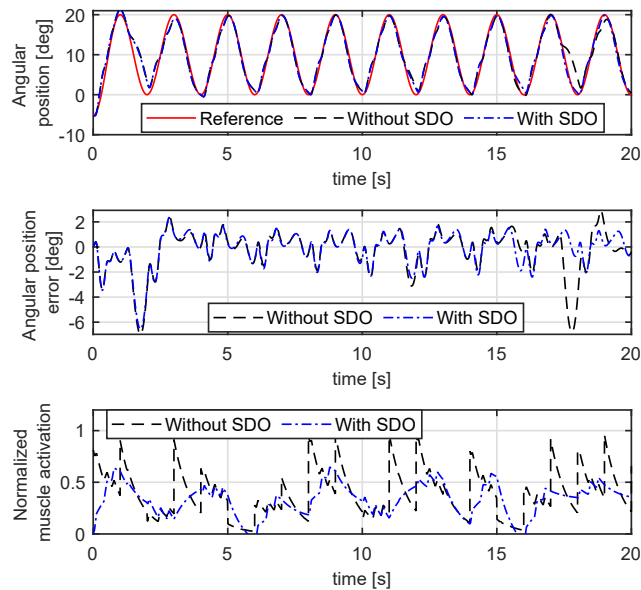


FIGURE 2. SIMULATION RESULTS OF THE CLOSED-LOOP SYSTEM WITH DSC-DC CONTROL (BASED ON THE SDO AND PURE SOLUTION OF MUSCLE ACTIVATION DYNAMICS).

5. SIMULATION RESULTS

To validate the SDO-DSC-DC controller for the FES-actuated ankle dorsiflexion neuromusculoskeletal system, simulations were conducted in Simulink with the fixed-step solver of 1 ms. As mentioned in Assumption 1, the signals θ and $\dot{\theta}$ were sampled at very high frequency 1000 Hz, so they were directly used as feedback in the closed-loop system synchronously with the solver. Preliminary real-time US imaging generation and processing study has been performed in our lab, and the average elapsed time for obtaining US imaging-derived muscle activation signal was around 1 second. Therefore, the US imaging-derived TA activation measurement was sampled at 1 Hz in simulation. The model parameters for the second-order ankle dorsiflexion dynamic model (1) and the first-order muscle activation dynamic model (2) used in the simulation were identified experimentally from an able-bodied subject based on the approach described in [33]. Typically, EMD for human lower limbs varies between the range of 30 ms and 100 ms [34]. In the controller design, EMD was set to be a constant 50 ms, while in the ankle dynamic model it was defined to be a time-varying value between 35 ms and 65 ms with the purpose to test the robustness of the proposed SDO-DSC-DC controller. The modeling uncertainties and external disturbance $d_1(t)$ in (1) and $d_2(t)$ in (2) are defined as a zero mean white noise with an standard deviation of 1 Nm and 0.5.

According to [35], the ankle dorsiflexion motion range during swing phase mainly located between 0° and 20° (the toe up direction is positive). Based on this, the desired ankle dorsi-

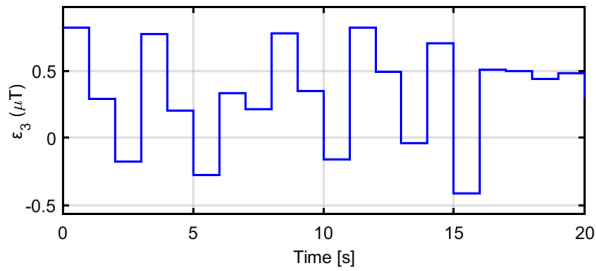


FIGURE 3. TA MUSCLE ACTIVATION UPDATE IN THE SDO BY USING US IMAGING-DERIVED DISCRETE MUSCLE ACTIVATION.

flexion trajectory was defined as a sinusoidal signal varying between this motion range with a frequency of 0.5 Hz and duration of 20 s. In the simulation, the control gains were designed as: $k = 50$, $\alpha_0 = 3$, $\alpha_1 = 1.2$, $k_1 = 5$, $k_2 = 20$, $\gamma = 1$, $\beta = 18.14$, and $\delta = 0.02$. Fig. 2 (a) presents the angular position tracking performance by using the proposed SDO-DSC-DC compared to the DSC-DC with pure solution of muscle activation dynamics, as depicted by centered blue line and dashed black line, respectively. The respective tracking errors are also shown in Fig. 2 (b), and the root mean square error (RMSE) is 1.38° vs. 1.72° , which indicates a improvement of 19.77 % by using SDO-DSC-DC. Random values between 0 and 1 were generated in Simulink every second to mimic the discrete muscle activation measurement coming from US imaging. Fig. 3 shows the update term in (6), which remains as a constant during the time interval of two successive US imaging-derived muscle activation measurements. In the simulation, the estimated muscle activation by using the SDO and the pure solution of muscle activation dynamics with US imaging-derived updated initial condition are shown in Fig. 2 (c). It is obvious that the muscle activation level is significantly lower by using SDO compared to the muscle activation calculated from sole dynamics. The findings imply that the proposed SDO-DSC-DC can achieve superior ankle dorsiflexion trajectory tracking performance, and at the same time reduce the muscle activation level, which is beneficial to suppress the undesired effects caused by muscle fatigue. Further investigation is needed to test the performance of muscle fatigue suppression by using the proposed control method.

6. CONCLUSION

In this paper, we proposed a trajectory tracking controller for a neuromusculoskeletal system with input delays and discrete muscle activation measure. A SDO was designed to continuously estimate the muscle activation level based on the discrete US imaging-derived muscle activation signal, while DSC was used to avoid the “explosion of terms” during the controller design. In addition, a DC technique was used to deal with the FES-induced input delay. Stability analysis was performed by using a

Lyapunov approach, which proved the SGUUB tracking performance. Simulation results showed the superior trajectory tracking performance by using SDO-DSC-DC compared to DSC-DC using only the solution of activation dynamics. The future work will investigate the observation of muscle fatigue and muscle activation at the same time based on the proposed SDO, as well as the experimental implementation and verification for the proposed observer-based DSC-DC controller on human ankle joint.

REFERENCES

- [1] Cornwall, M. W., and Mcpoil, T. G., 1994. “The Influence of Tibialis Anterior Muscle Activity on Rearfoot Motion during Walking”. *Foot Ankle Int.*, **15**(2), pp. 75–79.
- [2] Daubney, M. E., and Culham, E. G., 1999. “Lower-Extremity Muscle Force and Balance Performance in Adults Aged 65 Years and Older”. *Phys. Ther.*, **79**(12), pp. 1177–1185.
- [3] Stein, R. B., Bélanger, M., Wheeler, G., Wieler, M., Popović, D. B., Prochazka, A., and Davis, L. A., 1993. “Electrical systems for improving locomotion after incomplete spinal cord injury: An assessment”. *Arch. Phys. Med. Rehabil.*, **74**(9), pp. 954–959.
- [4] Granat, M. H., Maxwell, D. J., Ferguson, A. C., Lees, K. R., and Barbenet, J. C., 1996. “Peroneal stimulator: Evaluation for the correction of spastic drop foot in hemiplegia”. *Arch. Phys. Med. Rehabil.*, **77**(1), pp. 19–24.
- [5] Killeen, T., Easthope, C. S., Demkó, L., Filli, L., Lőrincz, L., Linnebank, M., Curt, A., Zörner, B., and Bolliger, M., 2017. “Minimum toe clearance: probing the neural control of locomotion”. *Sci. Rep.*, **7**(1), pp. 1–10.
- [6] Kantrowitz, A., 1960. “Electronic physiologic aids”. *Report of the Maimonides Hospital*, pp. 4–5.
- [7] Liberson, W., Holmquest, H., Scot, D., and Dow, M., 1961. “Functional electrotherapy: stimulation of the peroneal nerve synchronized with the swing phase of the gait of hemiplegic patients.”. *Arch. Phys. Med.*, **42**, pp. 101–105.
- [8] Everaert, D. G., Thompson, A. K., Su Ling Chong, S. L., and Stein, R. B., 2010. “Does Functional Electrical Stimulation for Foot Drop Strengthen Corticospinal Connections?”. *Neurorehabil. Neural Repair*, **24**(2), pp. 168–177.
- [9] Kluding, P. M., Dunning, K., O’Dell, M. W., Wu, S. S., Ginosian, J., Feld, J., and McBride, K., 2013. “Foot Drop Stimulation Versus Ankle Foot Orthosis After Stroke”. *Stroke*, **44**(6), pp. 1660–1669.
- [10] Liberson, W., 1961. “Functional electrotherapy: stimulation of the peroneal nerve synchronized with the swing phase of the gait of hemiplegic patients”. *Arch. Phys. Med.*, **42**, pp. 101–105.
- [11] Alibeji, N. A., Molazadeh, V., Dicianno, B. E., and Sharma, N., 2018. “A control scheme that uses dynamic postural

- synergies to coordinate a hybrid walking neuroprosthesis: Theory and experiments”. *Front. Neurosci.*, **12**, p. 159.
- [12] Alibeji, N. A., Molazadeh, V., Moore-Clingenpeel, F., and Sharma, N., 2018. “A muscle synergy-inspired control design to coordinate functional electrical stimulation and a powered exoskeleton: Artificial generation of synergies to reduce input dimensionality”. *IEEE Cont. Syst. Mag.*, **38**(6), pp. 35–60.
- [13] Alibeji, N., Kirsch, N., Farrokhi, S., and Sharma, N., 2015. “Further results on predictor-based control of neuromuscular electrical stimulation”. *IEEE Trans. Neural Syst. Rehabil. Eng.*, **23**(6), pp. 1095–1105.
- [14] Karafyllis, I., Malisoff, M., de Queiroz, M., Krstic, M., and Yang, R., 2015. “Predictor-based tracking for neuromuscular electrical stimulation”. *Int. J. Robust Nonlinear Control*, **25**(14), pp. 2391–2419.
- [15] Downey, R. J., Merad, M., Gonzalez, E. J., and Dixon, W. E., 2016. “The time-varying nature of electromechanical delay and muscle control effectiveness in response to stimulation-induced fatigue”. *IEEE Trans. Neural Syst. Rehabil. Eng.*, **25**(9), pp. 1397–1408.
- [16] Alibeji, N., Kirsch, N., and Sharma, N., 2015. “Dynamic surface control of neuromuscular electrical stimulation of a musculoskeletal system with activation dynamics and an input delay”. In Proc. of ACC, IEEE, pp. 631–636.
- [17] Alibeji, N., Kirsch, N., Dicianno, B. E., and Sharma, N., 2017. “A modified dynamic surface controller for delayed neuromuscular electrical stimulation”. *IEEE/ASME Trans. Mechatron.*, **22**(4), Aug, pp. 1755–1764.
- [18] Kirsch, N., Bao, X., Alibeji, N., Dicianno, B., and Sharma, N., 2018. “Model-based dynamic control allocation in a hybrid neuroprosthesis”. *IEEE Trans. Neural Syst. Rehabil. Eng.*, **26**(1), pp. 224–232.
- [19] Vigotsky, A. D., Halperin, I., Lehman, G. J., Trajano, G. S., and Vieira, T. M., 2018. “Interpreting signal amplitudes in surface electromyography studies in sport and rehabilitation sciences”. *Front. Physiol.*, **8**, p. 985.
- [20] Li, Z., Guiraud, D., Andreu, D., Benoussaad, M., Fattal, C., and Hayashibe, M., 2016. “Real-time estimation of fes-induced joint torque with evoked emg”. *J. Neuroeng. Rehabil.*, **13**(1), p. 60.
- [21] Zhang, Q., Kim, K., and Sharma, N., 2020. “Prediction of Ankle Dorsiflexion Moment by Combined Ultrasound Sonography and Electromyography”. *IEEE Trans. Neural Syst. Rehabil. Eng.*, **28**(1), pp. 318–327.
- [22] Sheng, Z., Sharma, N., and Kim, K., 2019. “Quantitative assessment of changes in muscle contractility due to fatigue during nmes: An ultrasound imaging approach”. *IEEE Trans. Biomed. Eng.*
- [23] Shen, Y., Zhang, D., and Xia, X., 2017. “Continuous observer design for a class of multi-output nonlinear systems with multi-rate sampled and delayed output measurements”. *Automatica*, **75**, pp. 127–132.
- [24] Zhang, Q., Sheng, Z., Kim, K., and Sharma, N., 2019. “Observer design for a nonlinear neuromuscular system with multi-rate sampled and delayed output measurements”. In Proc. Am. Control Conf., IEEE, pp. 872–877.
- [25] Karafyllis, I., and Krstic, M., 2011. “Nonlinear stabilization under sampled and delayed measurements, and with inputs subject to delay and zero-order hold”. *IEEE Trans. Autom. Control*, **57**(5), pp. 1141–1154.
- [26] Ahmed-Ali, T., Van Assche, V., Massieu, J.-F., and Dorleans, P., 2013. “Continuous-Discrete Observer for State Affine Systems With Sampled and Delayed Measurements”. *IEEE Trans. Automat. Contr.*, **58**(4), pp. 1085–1091.
- [27] Du, H., Qian, C., and Li, S., 2013. “Global stabilization of a class of uncertain upper-triangular systems under sampled-data control”. *Int. J. Robust Nonlinear Control.*, **23**(6), pp. 620–637.
- [28] Zhang, D., and Shen, Y., 2017. “Global output feedback sampled-data stabilization for upper-triangular nonlinear systems with improved maximum allowable transmission delay”. *Int. J. Robust Nonlinear Control*, **27**(2), pp. 212–235.
- [29] Sharma, N., Stegath, K., Gregory, C. M., and Dixon, W. E., 2009. “Nonlinear neuromuscular electrical stimulation tracking control of a human limb”. *IEEE Trans. Neural Syst. Rehabil. Eng.*, **17**(6), pp. 576–584.
- [30] Sharma, N., Gregory, C., Johnson, M., and Dixon, W., 2012. “Closed-loop neural network-based NMES control for human limb tracking”. *IEEE Trans. Control Syst. Technol.*, **20**(3), pp. 712–725.
- [31] Schauer, T., Negard, N. O., Previdi, F., Hunt, K. J., Fraser, M. H., Ferchland, E., and Raisch, J., 2005. “Online identification and nonlinear control of the electrically stimulated quadriceps muscle”. *Control Eng. Pract.*, **13**, pp. 1207–1219.
- [32] Liu, Y., Wang, Z., and Liu, X., 2006. “On global exponential stability of generalized stochastic neural networks with mixed time-delays”. *Neurocomputing*, **70**(1-3), pp. 314–326.
- [33] Popović, D., Stein, R., Oğuztörel, M., Lebedowska, M., and Jonić, S., 1999. “Optimal control of walking with functional electrical stimulation: a computer simulation study”. *IEEE Trans. Rehabil. Eng.*, **7**(1), pp. 69–79.
- [34] Cavanagh, P. R., and Komi, P. V., 1979. “Electromechanical delay in human skeletal muscle under concentric and eccentric contractions.”. *Eur. J. Appl. Physiol. Occup. Physiol.*, **42**(3), pp. 159–63.
- [35] Blaya, J., and Herr, H., 2004. “Adaptive Control of a Variable-Impedance Ankle-Foot Orthosis to Assist Drop-Foot Gait”. *IEEE Trans. Neural Syst. Rehabil. Eng.*, **12**(1), mar, pp. 24–31.